PAPER

Check for updates

DPD simulations on morphologies and structures of blank PLGA-*b*-PEG-*b*-PLGA polymeric micelles and docetaxel-loaded PLGA-*b*-PEG-*b*-PLGA polymeric micelles†

Mengyao Wang, Ye Lin, Jianxu Gao and Dongmei Liu 🄳 *

Dissipative particle dynamics (DPD) simulation was used to study the morphologies and structures of blank (no drug) poly(lactic-*co*-glycolic acid)-*b*-poly(ethylene glycol)-*b*-poly(lactic-*co*-glycolic acid) (PLGA-*b*-PEG-*b*-PLGA) polymeric micelles and the docetaxel (Dtx)-loaded PLGA-*b*-PEG-*b*-PLGA polymeric micelles. We focused on the influences of PLGA-*b*-PEG-*b*-PLGA copolymer concentration, composition, Dtx drug content and the shear rate on morphologies and structures of the micelles. Our simulations show that the PLGA-*b*-PEG-*b*-PLGA copolymers in the aqueous solutions could aggregate and form blank micelles while Dtx drug and PLGA-*b*-PEG-*b*-PLGA could aggregate and form drug-loaded micelles. Under different PLGA-*b*-PEG-*b*-PLGA concentrations and drug content, the blank and drug-loaded micelles are observed as spherical, onionlike, columnar, and lamellar structures. The onionlike structures are comprised of the PEG hydrophilic core, the PLGA hydrophobic middle layer, and the PEG hydrophilic shell. As the structure of micelles varies from a spherical core–shell structure to a core–middle layer–shell onionlike structure, the distribution of the Dtx drugs diffuses from the core to the PLGA middle layer of the aggregate. In addition, the drug release process of the Dtx-loaded micelles under shear flow is also simulated. And the results show that the spherical micelles turn into a columnar structure under a shear rate from 0.2 to 3.4. When the shear rate increases to 3.5, the Dtx drugs released gradually increase until all are released with time evolution. These findings illustrate the dependence of the structural morphologies on the detailed molecular parameters of PLGA-*b*-PEG-*b*-PLGA and Dtx.

1. Introduction

In recent decades, the polymeric micelles assembled from amphiphilic block copolymers in an aqueous environment have received more and more attention.[1–4] Polymeric micelles can be used to deliver various drugs including paclitaxel (Ptx), doxorubicin (DOX), docetaxel (Dtx), *etc.* anticancer agents. The polymeric micelles used as anticancer drug carriers not only show high stability *in vivo*, good biocompatibility, high drug loading, *etc.* advantages,[5,6] but also show excellent properties in the improvement of drug-targeted release and chemotherapeutic efficacy, and the reduction of toxic effects of drugs.[7,8] Although considerable attention has been focused on the polymeric micelles as drug carriers, an in-depth and thorough investigation of the structures and morphologies of drug-loaded polymeric micelles is still required.

School of Science, North China University of Science and Technology, Tangshan, 063210, P. R. China. E-mail: dmliu@ncst.edu.cn

Among various polymeric micelles, poly(lactic acid-*co*-glycolic acid)-*b*-poly(ethylene glycol) (PEG)-*b*-poly(lactic acid-*co*-glycolic acid) (PLGA) (PLGA-*b*-PEG-*b*-PLGA) polymeric micelles have attracted significant attention.[9–22] PLGA-*b*-PEG-*b*-PLGA copolymers are excellent biomedical materials that exhibit advantages such as being biocompatible, degradable, thermosensitive, easily controlled, *etc.*,[9] which in aqueous solutions could form micelles composed of a PEG hydrophilic outer shell and a hydrophobic inner core delivering drugs.[23,24] The ability of PLGA-*b*-PEG-*b*-PLGA to solubilize hydrophobic compounds is attributed to their core/shell structure. Experimental studies of drug-loading PLGA-*b*-PEG-*b*-PLGA polymeric micelles were extensively performed. For instance, Ding *et al.*[11–14] prepared a PLGA-*b*-PEG-*b*-PLGA formulation for carrying the DOX drugs. They found that because of the intramolecular and intermolecular interactions between hydrophobic blocks, the PLGA-*b*-PEG-*b*-PLGA drug-loaded systems exhibited long-lasting maintenance after subcutaneous injection *in vivo*, which differs from Pluronic F-127.[11] Khorshid *et al.*[25] explored the influence of the hydrophilic PEG block lengths on the phase behavior when the hydrophobic PLGA blocks lengths were fixed. They observed that the aggregate's structure changed from spherical core–shell

micelles to cylindrical structure and packing of cylinders with ranging the temperature. Cao et al.[26] prepared liposomal doxorubicin with a particle size of 75 nm and PLGA-b-PEG-b-PLGA triblock copolymers. They suggested that the interactions between liposomes and PLGA-b-PEG-b-PLGA micelles promote micelles gathering and form bigger aggregation.[26]

Due to using only experimental techniques is difficult to examine detailed information on the molecules distribution and the dynamic properties of the drug-loaded system. Computer simulation methods have been widely used to investigate drug encapsulation and drug release behavior. Among various computational simulation methods, dissipative particle dynamics (DPD) simulation is an efficient mesoscopic simulation method that is suitable for studying complex multiphase systems.[27,28] Researchers have successfully applied DPD to study the formation, drugs distribution and release process for the drug-loaded micelles.[29,30] Specifically, Guo et al.[31] investigated the formation of DOX-loaded DHA-His$_{10}$Lys$_{10}$ polymeric micelles through DPD simulations. It was shown that under a defined condition, the DOX drugs and the DHA-His$_{10}$-Lys$_{10}$ copolymers aggregated and formed micelles; DOX drugs were distributed homogeneously inside the vehicle matrix, the stabilizers' lysine segments absorbed on the surface of the vehicle. Yang et al.[4] adopted DPD simulations to explore the co-micellization behavior, drug distribution regularities, and dual pH/reduction-responsive drug release process of mixed micelles. Kuru et al.[32] employed coarse-grained DPD simulations to study morphology, drug encapsulation, and release of poly(ethylene glycol)–poly(lactic acid)–poly(ethylene glycol) (PEG–PLA–PEG) amphiphilic block copolymer system. However, there is a rare simulation report about PLGA-b-PEG-b-PLGA polymeric micelles as carriers for drug delivery.

Here, we investigate the effects of PLGA-b-PEG-b-PLGA copolymer concentration, composition, and Dtx drug content on the morphologies and structures of the blank (no drug) PLGA-b-PEG-b-PLGA polymeric micelles and Dtx-loaded PLGA-b-PEG-b-PLGA micelles through DPD simulations. The model is constructed based on our previous and other studies.[4,31,33–36] The results can help to understand the PLGA-b-PEG-b-PLGA drug-loaded system, which in turn assists in the design and preparation of the optimal drug-loaded polymeric micelles.

2. Method

Dissipative particle dynamics (DPD) is a coarse-grained simulation method that operates at the mesoscale, which was first proposed by Hoogerbrugge and Koelman[27] to study fluid mechanics problems in 1992. In a DPD procedure, a whole molecular may be divided into several segments, which are generally referred to as beads. In the study of drug-loaded systems, the objects often involve complex assemblies of multiple molecules that require a relatively long simulation. The all-atom molecular dynamics (MD) simulation is reluctant to meet the time and the space requirements, the DPD simulation could reduce computational significantly by conserving the detailed microstructural features of the drug-loaded and drug release system.[37] And the application of DPD simulation in

this field is relatively more mature.[38–52] Thus, we investigate the morphologies and structures of the blank PLGA-b-PEG-b-PLGA polymeric micelle and the Dtx-loaded PLGA-b-PEG-b-PLGA polymeric micelle by DPD simulations.

2.1 Model

In DPD simulation, the motion of all beads is governed by Newton's equations of motion.[53]

The force acting on a bead i complies with Newton's second law,

$$\frac{d\mathbf{r}_i}{dt} = \mathbf{v}_i; \quad m_i\frac{d\mathbf{v}_i}{dt} = \mathbf{F}_i \tag{1}$$

where $\mathbf{r}_i$, $\mathbf{v}_i$ and m_i refer to the position vector, velocity vector, and mass of bead i, respectively. For simplicity, the masses of all beads are set to 1 DPD unit. The force $\mathbf{F}_i$ exerted on bead i is the sum of the conservative force $\mathbf{F}_{ij}^C$, the dissipative force $\mathbf{F}_{ij}^D$, the random force $\mathbf{F}_{ij}^R$ and the harmonic spring force $\mathbf{F}_i^S$

$$\mathbf{F}_i = \sum_{j \neq i}\left(\mathbf{F}_{ij}^C + \mathbf{F}_{ij}^D + \mathbf{F}_{ij}^R\right) + \mathbf{F}_i^S \tag{2}$$

The conservative force $\mathbf{F}_{ij}^C$ is a soft repulsion force, which is given by[38]

$$\mathbf{F}_{ij}^C = \begin{cases} \alpha_{ij}(1 - r_{ij})\mathbf{e}_{ij} & (r_{ij} < 1) \\ 0 & (r_{ij} \geq 1) \end{cases} \tag{3}$$

where α_{ij} denotes the interaction parameter referred to the maximum repulsive magnitude of different beads. r_{ij} is the distance between the position of beads i and j, which is the absolute value of the vector $\mathbf{r}_{ij} = \mathbf{r}_i - \mathbf{r}_j$, i.e., $r_{ij} = |\mathbf{r}_{ij}|$, and $\mathbf{e}_{ij} = \mathbf{r}_{ij}/r_{ij}$ is the unit vector of $\mathbf{r}_{ij}$.

The dissipative force $\mathbf{F}_{ij}^D$ and the random force $\mathbf{F}_{ij}^R$ are given by

$$\mathbf{F}_{ij}^D = -\gamma\omega^D(r_{ij})(\mathbf{v}_{ij}\cdot\mathbf{e}_{ij})\mathbf{e}_{ij} \tag{4}$$

$$\mathbf{F}_{ij}^R = \sigma_{ij}\omega^R(r_{ij})\xi_{ij}\Delta t^{-1/2}\mathbf{e}_{ij} \tag{5}$$

where $\mathbf{v}_{ij} = \mathbf{v}_i - \mathbf{v}_j$ and γ are the velocity difference of beads i and j and the friction coefficient, respectively; σ_{ij} controls the magnitude of the random force; the random number ξ_{ij} has unit variance and zero average; the functions $\omega^D(r_{ij})$ and $\omega^R(r_{ij})$ are two distance-dependent weight functions, which comply with the fluctuation–dissipation theorem[53]

$$\omega^D(r_{ij}) = [\omega^R(r_{ij})]^2, \quad \sigma_{ij}^2 = 2\gamma k_B T \tag{6}$$

where k_B is the Boltzmann constant and T is the simulation temperature. According to Groot and Warren,[53] $\omega^D(r_{ij})$ and $\omega^R(r_{ij})$ follow relation

$$\omega^D(r_{ij}) = [\omega^R(r_{ij})]^2 = \begin{cases} (1 - r_{ij})^2 & (r_{ij} < 1) \\ 0 & (r_{ij} \geq 1) \end{cases} \tag{7}$$

The repulsive parameter values α_{ij} of different types of beads follow relationship[53]

$$\alpha_{ij} \approx \alpha_{ii} + 3.27\chi_{ij} \qquad (8)$$

In this relationship, χ_{ij} is the Flory–Huggins parameter, α_{ii} is the interaction of the same types of beads, which follows relation[53,54]

$$\alpha_{ii} = k_B T \frac{k^{-1} N_m - 1}{2\alpha \rho_{DPD}} \qquad (9)$$

where $k_B T = 1$, the dimensionless compressibility $k^{-1} = 15.9835$ at room temperature. N_m is the water molecule number of consisting a coarse-grained water bead. $\alpha = 0.101 \pm 0.001$; ρ_{DPD} is the number density of the system, thus the repulsion parameters $\alpha_{ii} = 78$.

Here, the Flory–Huggins parameter χ_{ij} can be calculated according to the following equation[55]

$$\chi_{ij} = \frac{(\delta_i - \delta_j)^2 V_{bead}}{RT} \qquad (10)$$

where δ_i and δ_j are the solubility parameters of beads i and j, V_{bead} is the average molar volumes of all beads, the gas constant $R \approx 8.314$. The solubility parameter can be calculated by molecular dynamics simulations from the chemical structure of the molecular fragments.[31]

The harmonic spring force $\mathbf{F}_i^S$ can be calculated by the following relationship with spring force constant $C = 4.0$ (ref. 28).

$$\mathbf{F}_i^S = \sum_{j \neq i} C\mathbf{r}_{ij} \qquad (11)$$

2.2 Simulation details

The DPD simulations are performed in a $20 \times 20 \times 20$ cubic box using Materials Studio with Periodic boundary conditions. It should be noted that the previous simulations have proved that this box is sufficient to avoid the finite-size effects.[56] The simulations are accomplished in the NVT ensemble. The simulation temperature $k_B T = 1$, the bead density $\rho = 3$, the friction coefficient $\gamma = 4.5$, the cutoff radius $r_c = 1$, these conditions ensured the simulations could relax reasonably and efficiently. In initial configurations, all components are randomly placed in the simulation box. The simulation initially runs for 2×10^5 steps with a time step $\Delta t = 0.05$ to achieve thermodynamic equilibrium.

In this work, the components comprised of PLGA-*b*-PEG-*b*-PLGA copolymer, Dtx drug, and water. Docetaxel (Dtx) is widely used in cancer treatment selected as the model drug. In the PLGA-*b*-PEG-*b*-PLGA triblock copolymer, PLGA is the hydrophobic block, PEG is the hydrophilic block. Simple coarse-grained models of components are used in this study. In order to ensure that there is no problem with the model, we referred to the studies of Cao *et al.*[57] and Zhou *et al.*[58] to divide the molecular structure, which is shown in Fig. 1. Several atoms or a functional group are represented as a DPD bead that is highlighted by color. The PLGA-*b*-PEG-*b*-PLGA[59] is separated into L (green), G (yellow), and E (blue) beads; the Dtx drug is divided into D1 (pink), D2 (pink), D3 (pink) beads; three
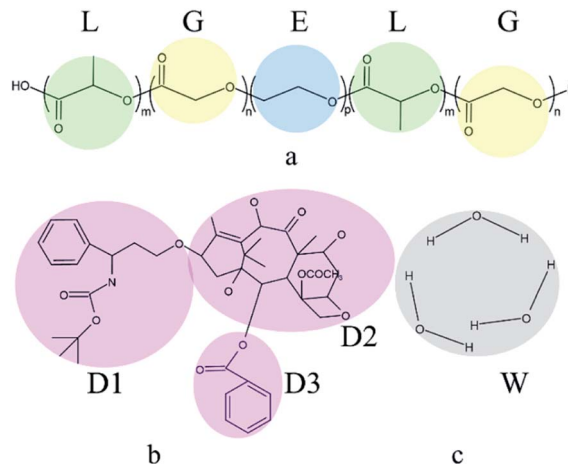

Fig. 1 Coarse graining of the simulated system. (a) PLGA-*b*-PEG-*b*-PLGA, (b) docetaxel, (c) water.

Table 1 Interaction parameter between beads

	L	G	E	D1	D2	D3	W
L	78.00						
G	78.04	78.00					
E	82.96	81.76	78.00				
D1	79.65	78.98	81.95	78.00			
D2	78.15	78.01	88.43	79.50	78.00		
D3	78.83	78.45	80.55	78.02	78.87	78.00	
W	161.3	149.3	114.0	222.3	288.3	161.6	78.00

molecules of water are represented as a bead W (grey). The number of L and G beads in the PLGA block is equal. We set the interaction parameters of different types of beads according to the ref. 57 and 58, which are shown in Table 1.

3. Results and discussion

3.1 The morphologies and structures of blank PLGA-*b*-PEG-*b*-PLGA micelles

In order to investigate the aggregation and distribution behavior of the Dtx drugs in the PLGA-*b*-PEG-*b*-PLGA micelles, the DPD simulations on the blank PLGA-*b*-PEG-*b*-PLGA micelles were initially carried out. The PLGA$_3$-*b*-PEG$_7$-*b*-PLGA$_3$ is chosen according to a real PLGA$_{1200}$-*b*-PEG$_{1450}$-*b*-PLGA$_{1200}$ copolymer,[59] by the relationship[60]

$$N_{DPD} = \frac{M_p}{M_m C_n} \qquad (12)$$

where M_p and M_m represent the molecular weight of polymer and monomer, respectively. The characteristic ratio C_n could be calculated by the Synthia module in Materials Studio.

3.1.1 Formation of blank PLGA-*b*-PEG-*b*-PLGA micelles. The PLGA-*b*-PEG-*b*-PLGA copolymers were predicted to form core–shell spherical micelles in an aqueous solution.[23,24] To better understand the formation of the PLGA-*b*-PEG-*b*-PLGA micelles, we analyzed the morphologies evolution of the blank

PLGA-*b*-PEG-*b*-PLGA micelles during one DPD simulation. Fig. 2 and S1† show the representative morphology snapshots and the radial distribution functions for the PLGA-*b*-PEG-*b*-PLGA and water system at different simulation steps. The system is composed of 10% PLGA$_3$-*b*-PEG$_7$-*b*-PLGA$_3$ copolymer beads and 90% water beads. In the morphology snapshots, the water beads were hidden so as to show the morphologies of the aggregates more clearly.

Fig. 2 shows the micellization process of PLGA$_3$-*b*-PEG$_7$-*b*-PLGA$_3$ in an aqueous solution is similar to that of most other polymeric micelles.[4,31] Specifically, at the beginning of the simulation, *i.e.* $t = 0$ steps, all copolymers are randomly mixed, the PLGA$_3$-*b*-PEG$_7$-*b*-PLGA$_3$ copolymers exhibit a disordered state [Fig. 2a]. With the evolution of simulation, at $t = 1000$ steps, we see some PLGA$_3$-*b*-PEG$_7$-*b*-PLGA$_3$ copolymers have aggregated and formed clusters for the intermolecular interactions, as shown by [Fig. 2b]. With further increasing the simulation time to $t = 10\,000$ steps, the smaller PLGA$_3$-*b*-PEG$_7$-*b*-PLGA$_3$ clusters merge and form big aggregates [Fig. 2c]. As the simulation progresses, due to the attractive interaction of the aggregates, the aggregates will further grow and form larger aggregates [Fig. 2d $t = 30\,000$ steps]. In the final state $t \geq 50\,000$ steps [Fig. 2e and f], all PLGA$_3$-*b*-PEG$_7$-*b*-PLGA$_3$ copolymer chains are closely combined and form a stable and complete spherical polymeric micelle, which is consistent with a spherical single-core micelle reported in early research.[9] These results indicate that the formative process of the blank PLGA-*b*-PEG-*b*-PLGA micelles is an evolution from disordered to the ordered state of distributions of PLGA-*b*-PEG-*b*-PLGA copolymers. The hydrophobic PLGA blocks and hydrophilic PEG blocks in an aqueous solution could separate spontaneously. The core of the PLGA-*b*-PEG-*b*-PLGA micelle provides the loading space for hydrophobic drugs (*e.g.* Dtx, DOX), the hydrophilic PEG shell of the micelles exhibits a stabilizing and dispersing effect. Since we have demonstrated that the PLGA-*b*-PEG-*b*-PLGA copolymers in an aqueous solution indeed form a micelle, we next focus on exploring the effects of the PLGA-*b*-PEG-*b*-PLGA copolymer

concentration and composition on the morphologies and structures of the micelle.

To examine whether the system achieves an equilibrium state or not, the time evolutions of the radial distribution functions for the beads of the PLGA-*b*-PEG-*b*-PLGA copolymers were investigated. The results are displayed in Fig. S1.† In the initial state $t = 0$, PLGA-*b*-PEG-*b*-PLGA copolymers and water are randomly mixed, the curve shows a low peak at $r < 1$, which indicates that the interactions between the PLGA$_3$-*b*-PEG$_7$-*b*-PLGA$_3$ beads are weak [the black solid line of $g_{cc}(r)$ in Fig. S1†]. With the time evolution t increase from 1000 to 30 000, due to the significantly aggregate, the width and height of the peak exhibit an increase [the LT magenta dash line, the blue dash-dot line, the orange dash-dot line of $g_{cc}(r)$ in Fig. S1†]. In the final state, the width and height of the peak of $g_{cc}(r)$ in Fig. S1† almost no change, which indicates that the systems have reached equilibration.

3.1.2 Effect of PLGA$_3$-*b*-PEG$_7$-*b*-PLGA$_3$ copolymer concentration. To investigate how the PLGA-*b*-PEG-*b*-PLGA concentration c_{cp} influences the micelles' morphologies and structures, DPD simulations on the PLGA$_3$-*b*-PEG$_7$-*b*-PLGA$_3$ concentration c_{cp} ranging from 2.5% to 40% were carried out. To show the structures clearly, sectional views of self-assembled morphologies also are displayed. Fig. 3 shows the morphologies (a1–h1) and their sectional views (a2–h2) for the PLGA$_3$-*b*-PEG$_7$-*b*-PLGA$_3$ with different copolymer concentrations c_{cp}. The corresponding density distributions with E, L, G beads are shown in Fig. S2.† It can be seen that PLGA$_3$-*b*-PEG$_7$-*b*-PLGA$_3$ copolymers in an aqueous solution can self-assemble into micelle at a lower copolymer concentration of $c_{cp} = 2.5\%$ [Fig. 3a1 and a2], which is because of the strong hydrophobicity of the PLGA blocks. When the concentration of PLGA$_3$-*b*-PEG$_7$-*b*-PLGA$_3$ copolymer $c_{cp} \leq 15\%$, the E, L, G beads enrich around 10 [Fig. S2a–e†], all PLGA$_3$-*b*-PEG$_7$-*b*-PLGA$_3$ beads are closely combined in the aqueous solution and formed a spherical micelle[11] [Fig. 3a1–e1]. However, the microstructure of the micelles varies significantly. Specifically, as the PLGA$_3$-*b*-PEG$_7$-*b*-PLGA$_3$ copolymer concentration is increased from $c_{cp} = 2.5\%$ to 5% [Fig. S2a and b†], the hydrophobic beads L and G of the PLGA block aggregate inside E beads form the hydrophobic core of the micelle, the E beads of the PEG blocks arrange orderly around the L and G beads and form the shell of the spherical micelle [Fig. 3a2 and b2]. As the PLGA$_3$-*b*-PEG$_7$-*b*-PLGA$_3$ copolymer concentration c_{cp} increased from $c_{cp} = 7.5\%$ to $c_{cp} = 15\%$ [Fig. S2c–e†], the densities of the E beads at the core close to the densities of the L and G beads, indicating onionlike structures[61] were formed, with the hydrophilic PEG core, the PLGA hydrophobic middle layer, and the PEG hydrophilic shell [Fig. 3c2–e2]. This core–middle layer–shell onionlike micelle looks similar to the normal core–shell spherical micelles from the outside. Fig. S2a–e† also shows that the size of the micelle increases with increasing the PLGA$_3$-*b*-PEG$_7$-*b*-PLGA$_3$ concentration. Fig. S3† describes the size of the spherical micelles at different copolymer concentrations. We found that as the concentration increases from $c_{cp} = 2.5\%$ to $c_{cp} = 15\%$, the size of the spherical micelles increases from 2.775 nm to 5.009 nm [the black solid square in Fig. S3†], which is close to the DPD simulation size of the PLA–PEG–PLA
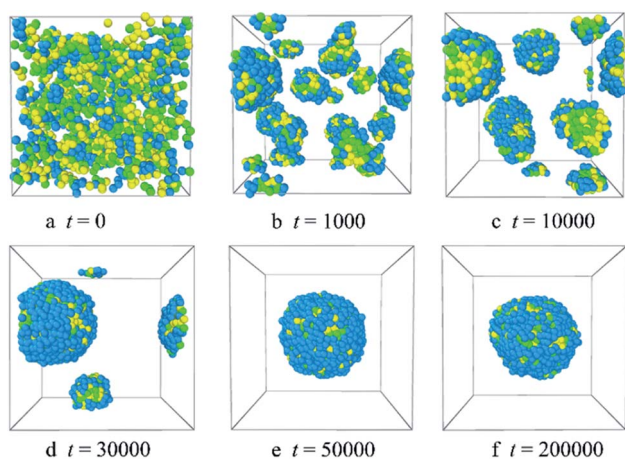

Fig. 2 Representative morphology snapshots of the blank PLGA$_3$-*b*-PEG$_7$-*b*-PLGA$_3$ micelles at different simulation times. Green, yellow and blue spheres represent beads L, G, and E respectively.
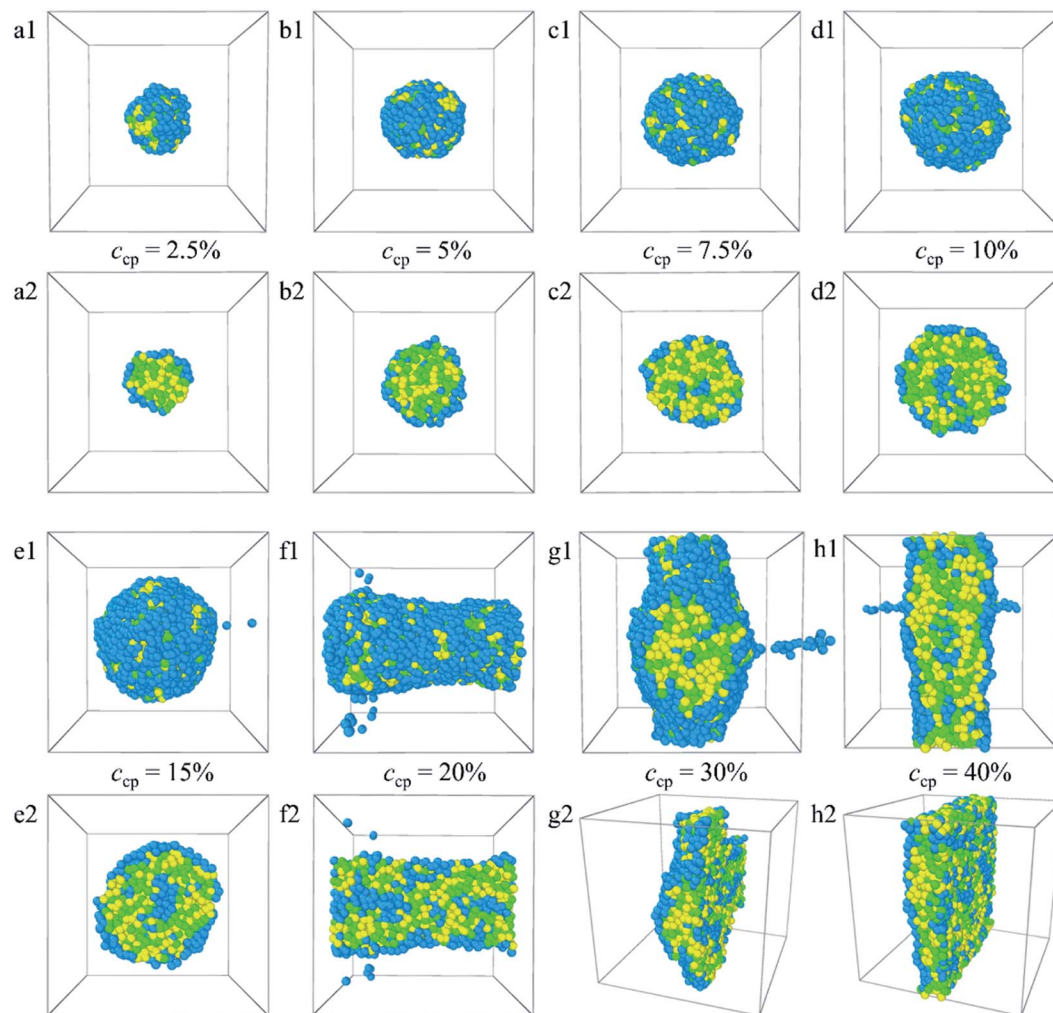
Fig. 3 Morphology snapshots (a1–h1) and their sectional views (a2–h2) of the blank PLGA$_3$-*b*-PEG$_7$-*b*-PLGA$_3$ micelles with different copolymer concentrations. The green, yellow and blue spheres represent beads L, G, and E respectively.

copolymer micelle by Chansuna *et al.*[62] Though this size is less than the experiment size of 20–40 nm, the trend is in qualitative agreement with the experimental results of Khodaverdi *et al.*[16] This result is because the micelle size in DPD simulations is dependent on the system size, the side length of our simulation box is $20 \times r_c$(0.65 nm) = 13 nm, thus the micelle size of the simulation is less than the experiment value. However, as the PLGA$_3$-*b*-PEG$_7$-*b*-PLGA$_3$ concentration increases to c_{cp} = 20% [Fig. S2f†], the E, L, G beads have the widest distribution, and the density curves fluctuate around 0.2, corresponding to the columnar structure[25] [Fig. 3f1 and f2]. When the c_{cp} further increases from 30% to 40%, the distribution of the E, L, G beads narrows again, the E beads are distributed on both sides of the L and G beads [Fig. S2g and h†], which is consistent with the lamellar structure[31] [Fig. 3g1–h2].

From the analyses made above, it is known that when the PLGA$_3$-*b*-PEG$_7$-*b*-PLGA$_3$ copolymer concentration c_{cp} constantly increases, the interactions between the beads change the structure of micelles from normal spherical to onionlike to columnar to lamellar. The structural changes ensure

a minimum contacting area between the hydrophobic groups and water, thus keeping the system stable.

3.1.3 Effect of PEG ratio. Here, we increase the ratio of PEG by increasing the length of the PEG block from N_{PEG} = 3 to 9 by fixing the block length of the copolymer. The PLGA-*b*-PEG-*b*-PLGA copolymers concentration c_{cp} = 10%. Fig. 4 shows the dependence of morphologies and their sectional views for the PLGA-*b*-PEG-*b*-PLGA micelles on the PEG block lengths. The corresponding density distributions with E, L, G beads of the PLGA-*b*-PEG-*b*-PLGA are shown in Fig. S4.† In Fig. S4,† it is found that the E, L, G beads enrich around 10, the PLGA-*b*-PEG-*b*-PLGA copolymers aggregate and form a spherical micelle at all PEG block lengths [Fig. 4]. As the PEG block content is lower N_{PEG} = 3 [Fig. 4a1, a2 and S4a†], the PLGA-*b*-PEG-*b*-PLGA copolymers in an aqueous solution can self-assemble into core–shell micelle, all PEG beads aggregate at the shell of the micelle, the E beads are too little and couldn't completely cover the shell of the micelle, there are many L and G beads exposed at the shell. As the PEG block length increases to N_{PEG} = 5 [Fig. S4b†], the E beads enriched outside the L and G beads increase,
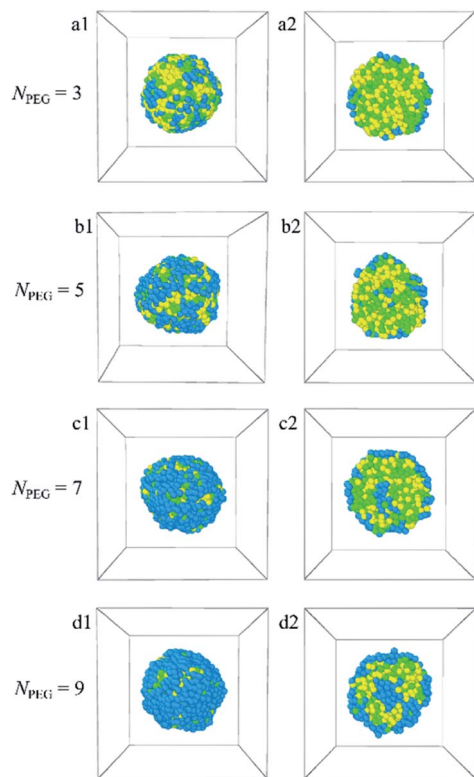
Fig. 4 Morphology snapshots (a1–d1) and their sectional views (a2–d2) of the blank PLGA-*b*-PEG-*b*-PLGA micelles with different PEG block lengths. The green, yellow and blue spheres represent beads L, G, and E respectively.
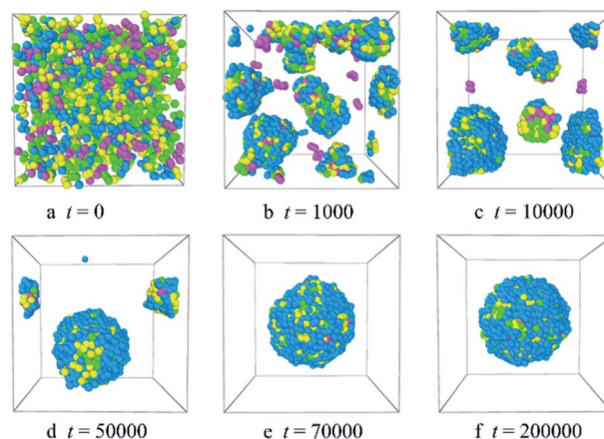

Fig. 5 Representative morphologies of Dtx-loaded PLGA$_3$-*b*-PEG$_7$-*b*-PLGA$_3$ micelles at different simulation times. The green, yellow and blue spheres represent beads L, G, and E respectively, and the pink spheres represent beads D1, D2, and D3 of the Dtx drug.

indicating the E beads that covered the shell increase [Fig. 4b1], and though the E beads still can't completely cover the L and G beads of PLGA, there are a few E beads distributed at the center of the micelle and form the core, the L and G beads of PLGA blocks form the hydrophobic middle layer, the remaining most PEG beads form the shell of the micelle, *i.e.* an onionlike structure is formed [Fig. 4b2]. With the PEG block lengths further increasing from $N_{PEG} = 7$ to 9 [Fig. 4c1, c2 and S4c, d†], the E beads covering the shell increase, the L and G beads exposed at the shell decrease, the E beads distributed at the core of the onionlike structure increase [Fig. 4d1 and d2]. These findings suggest that the blank PLGA-*b*-PEG-*b*-PLGA polymeric micelle undergoes a transition from spherical (core–shell) to onionlike (core–middle layer–shell) structure with increasing the PEG ratio.

3.2 The morphologies and structures of the Dtx-loaded polymeric micelles

3.2.1 Formation of the Dtx-loaded PLGA-*b*-PEG-*b*-PLGA micelles.
For a clearer analysis of the evolution of the PLGA-*b*-PEG-*b*-PLGA drug delivery system, we explore the conformation and the radial distribution functions of Dtx-loaded PLGA-*b*-PEG-*b*-PLGA micelles in an aqueous solution at different simulation times, as illustrated in Fig. 5 and S5.† The system is composed of 10% PLGA$_3$-*b*-PEG$_7$-*b*-PLGA$_3$, 2% Dtx drug, and 88% water. At $t = 0$ steps, the simulation system is in

a disordered and homogeneous state [Fig. 5a and the black solid line of $g_{cc}(r)$ in Fig. S5†]. With the evolution of simulation at $t = 1000$ steps, as shown by Fig. 5b, due to the repulsive interaction between the PLGA, Dtx and water, some PLGA$_3$-*b*-PEG$_7$-*b*-PLGA$_3$ copolymers and the Dtx beads aggregate and form many small clusters, corresponding to the LT magenta dash line of $g_{cc}(r)$ in Fig. S5,† the width and height of the peak exhibit an obvious increase. The clusters forming exhibit the following characteristics: the hydrophobic Dtx beads are distributed inside the clusters, the PLGA$_3$-*b*-PEG$_7$-*b*-PLGA$_3$ copolymers adsorb on the surface of the clusters. We inferred that the reason for forming these clusters is that the Dtx drugs and the PLGA blocks are both hydrophobic which causes them to aggregate in an aqueous solution, whereas the PEG blocks are hydrophilic which causes them to surround the hydrophobic beads. As the simulation times increase to $t = 10\,000$ steps [Fig. 5c], the small clusters gather into several clusters with big size, which corresponds to the blue dash-dot line of $g_{cc}(r)$ in Fig. S5,† the curve shows a broader and higher peak. Meanwhile, most of the Dtx drug beads are absorbed inside the PLGA$_3$-*b*-PEG$_7$-*b*-PLGA$_3$ micelles, and a very little left of Dtx drug beads are still dispersed in the aqueous solution. With further increase the simulation steps to $t = 50\,000$ [Fig. 5d], the adjacent micelles can further gather and form larger micelles and the free Dtx drug beads were all diffused into the spherical micelle, which results in the increases of the width and height of the peak [the orange dash-dot line of $g_{cc}(r)$ in Fig. S5†]. That is, as the size of the clusters increases to a certain extent, the morphologies of the aggregates would change from formless structure to spherical structure, *i.e.* the spherical drug-loaded micelles. As the simulation steps increase to $t = 70\,000$ [Fig. 5e], all the micelles conglomerate and form a stable and complete spherical micelle. All Dtx drug beads are distributed inner of the micelle with PEG blocks adsorbed on the outer surface of the micelle. This indicates that the Dtx drugs could be well encapsulated inside the PLGA$_3$-*b*-PEG$_7$-*b*-PLGA$_3$ micelles. After that, when the simulation steps further increase to $t = 200\,000$, the

morphology and size of the spherical micelle and the radial distribution profiles almost no change which suggested that the microphase separation of this system had reached a dynamic equilibrium [Fig. 5f and S5†]. In comparison with the formation process of blank $PLGA_3$-b-PEG_7-b-$PLGA_3$ micelles, the Dtx-loaded $PLGA_3$-b-PEG_7-b-$PLGA_3$ micelles require more steps to reach equilibrium.

3.2.2 Effect of $PLGA_3$-b-PEG_7-b-$PLGA_3$ copolymer concentration. Fig. 6 shows the aggregate morphologies (a1–h1) and their sectional views (a2–h2) of the Dtx-loaded $PLGA_3$-b-PEG_7-b-$PLGA_3$ micelle at different copolymer concentrations. The content of $PLGA_3$-b-PEG_7-b-$PLGA_3$ copolymer and Dtx drug is fixed at 5 : 1. The corresponding density distributions with E, L, G, and Dtx drug beads are shown in Fig. S6.† We found that all the Dtx drugs and $PLGA_3$-b-PEG_7-b-$PLGA_3$ copolymers aggregate together, whereas the morphologies and structures vary significantly with copolymer concentration. Specifically, as the concentration of the $PLGA_3$-b-PEG_7-b-$PLGA_3$ copolymer $c_{cp} < 10\%$ [Fig. 6a1–c1 and S6a–c†], the E beads mainly distributed on

the outermost layer form the shell of the micelle, all Dtx drug beads are distributed at the center of the micelle and form the hydrophobic core of the micelle [Fig. 6a2–c2], which indicates that a core–shell spherical micelle is formed in the system. This result is supported by the experimental observations of Gao *et al.*[19] Meanwhile, the size of the micelle increases with increasing the $PLGA_3$-b-PEG_7-b-$PLGA_3$ copolymer concentration [the red solid dot in Fig. S3†].[16] As the concentration of the $PLGA_3$-b-PEG_7-b-$PLGA_3$ copolymers increases to $c_{cp} = 10\%$ [Fig. S6d†], the density of E beads at the center of the micelle increases, the onionlike structure[61] is formed [Fig. 6d1 and d2]. This onionlike structure is comprised of the hydrophilic PEG core, the PLGA hydrophobic middle layer, and the PEG hydrophilic shell [Fig. 6d2]. The Dtx drug beads are distributed at the PLGA middle layer. As the $PLGA_3$-b-PEG_7-b-$PLGA_3$ copolymers concentration increases to $c_{cp} = 15\%$ and 20% [Fig. S6e and f†], the densities of all the E, L, G, Dtx beads along the x-axis are all significantly greater than 0 and fluctuate around a certain value, the structure of the Dtx-loaded $PLGA_3$-b-PEG_7-b-$PLGA_3$ micelle
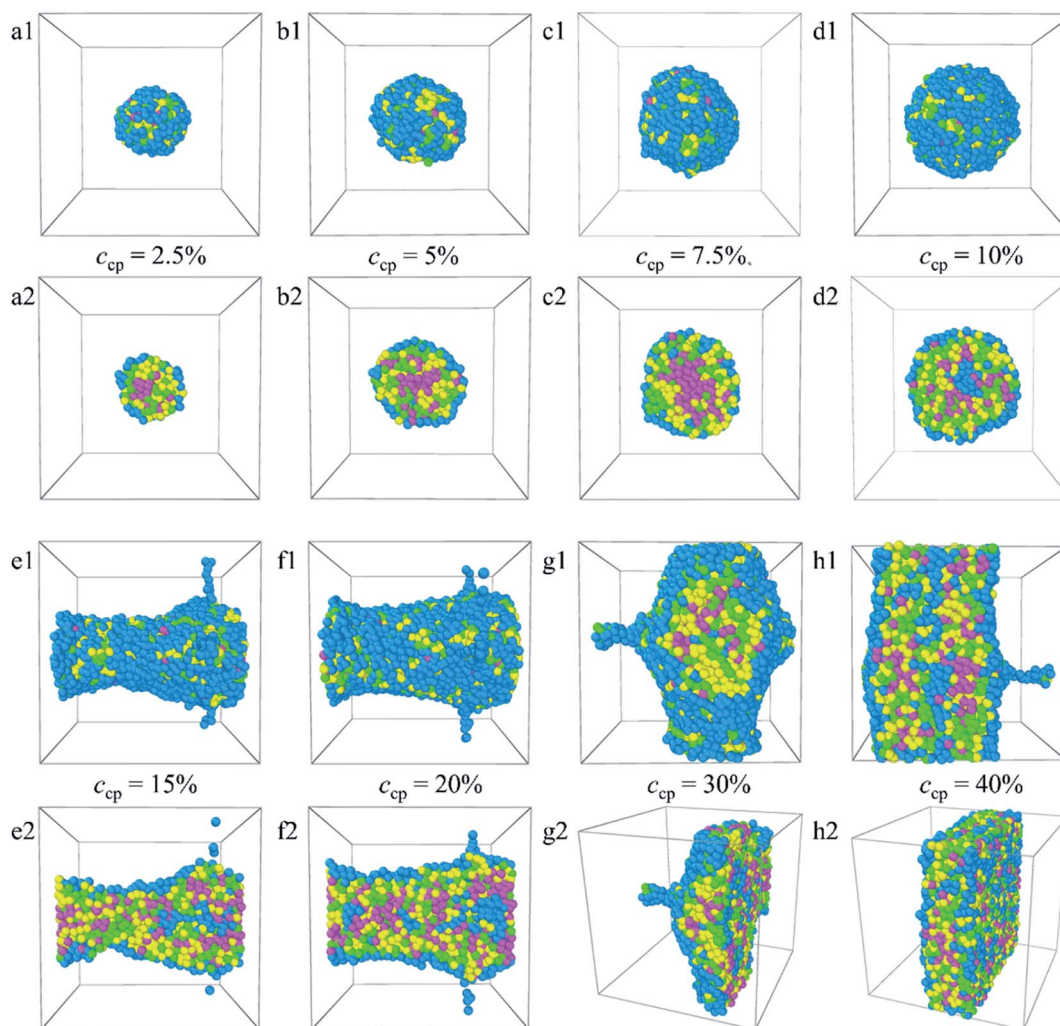

Fig. 6 Morphology snapshots (a1–h1) and their sectional view (a2–h2) of Dtx-loaded $PLGA_3$-b-PEG_7-b-$PLGA_3$ micelles with different copolymer concentrations. The green, yellow and blue spheres represent beads L, G, and E respectively, and the pink spheres represent beads D1, D2, and D3 of the Dtx drug.

© 2022 The Author(s). Published by the Royal Society of Chemistry

has a significant change from spherical structure to columnar structure[25] [Fig. 6e1–f2]. A lamellar structure[31] is gradually formed when the concentration of PLGA$_3$-b-PEG$_7$-b-PLGA$_3$ copolymers is further increased to c_{cp} = 30% and 40% [Fig. 6g1–h2 and S6g, h†]. These structures ensure a minimum contacting area of the hydrophobic L, G, D1, D2, D3 beads and water beads W, thus maintaining the stability of the system.

3.2.3 **Effect of PEG ratio.** To investigate the effect of the PEG ratio, the length of the PEG block is increased from N_{PEG} = 3 to 9 in fixed the block length of the copolymer. Fig. 7 shows the dependence of the morphology snapshots (a1–d1) and their sectional views (a2–d2) of Dtx-loaded PLGA-b-PEG-b-PLGA micelles on the PEG block lengths. The PLGA-b-PEG-b-PLGA copolymers concentration c_{cp} = 10%. The corresponding density distributions with the E, L, G beads of the PLGA-b-PEG-b-PLGA copolymers and the Dtx beads are shown in Fig. S7.† In Fig. S7,† it is found that the E, L, G, and Dtx beads all enriched around 10, corresponding to the spherical micelle [Fig. 7a1–d1]. As the PEG block lengths are short N_{PEG} = 3 and 5 [Fig. 7a1, b1 and S7a, b†], the E beads are too little and can't pack hydrophobic PLGA and Dtx drug completely, which results in a micelle with less stability. It should be noted that though PEG blocks can't pack hydrophobic PLGA and Dtx drug completely, there is a small amount of PEG beads are distributed at the core [Fig. 7a2 and b2]. As the PEG block lengths increase to N_{PEG} = 7

and 9 [Fig. S7c and d†], the density curves of the E beads rise, indicating the E beads covering the shell increase [Fig. 7c1 and d1]. The E beads distributed at the center of the micelles increase and form the hydrophilic PEG core, the L and G beads form the hydrophobic middle layer, the remaining E beads form the shell of the micelle, forming a core–middle layer–shell onionlike structure [Fig. 7c2 and d2]. It should be noted that as N_{PEG} = 9, the ratio of PLGA decreases, the formed PEG shell becomes thicker, whereas the PLGA core becomes smaller, which leads to the content of drug-loaded will also decrease. Therefore, too thick the PEG shell layer is also unnecessary, just cover the surface to a certain thickness. These results indicate that the structures of the Dtx-loaded PLGA-b-PEG-b-PLGA micelle also depend strongly on the PEG ratio. To moderate the micelle's drug loading efficiency (a small PLGA core will load a small amount of hydrophobic anticancer drug Dtx) and stability (a thin PEG shell may make the core–shell micelle unstable), PLGA-b-PEG-b-PLGA copolymer with the PEG block length N_{PEG} = 7 is considered to be the best drug carrier candidate.

3.2.4 **Effect of Dtx drug content.** Guo *et al.* have reported that there should be a limit to the capacity of the micelle-loading drug molecules.[31] In order to verify the argument, the morphologies snapshots (a1–h1) and their sectional views (a2–h2) of the Dtx-loaded PLGA$_3$-b-PEG$_7$-b-PLGA$_3$ micelles at
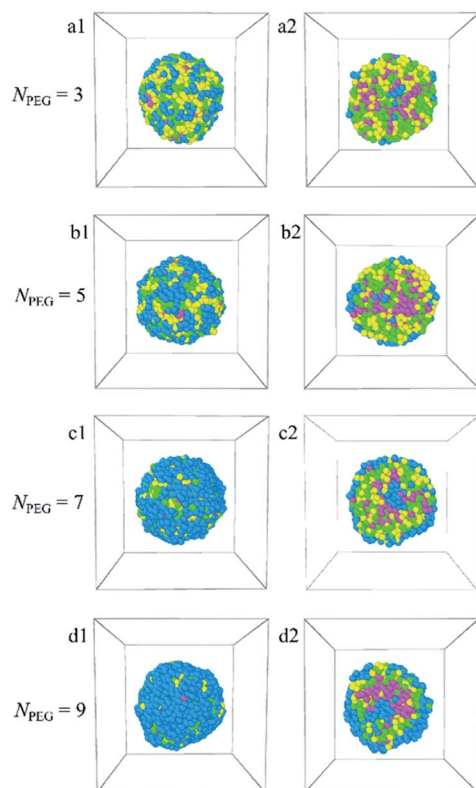

Fig. 7 Morphology snapshots (a1–d1) and their sectional view (a2–d2) of Dtx-loaded PLGA-b-PEG-b-PLGA micelles with different PEG blocks lengths. The green, yellow and blue spheres represent beads L, G, and E respectively, and the pink spheres represent beads D1, D2, and D3 of the Dtx drug.
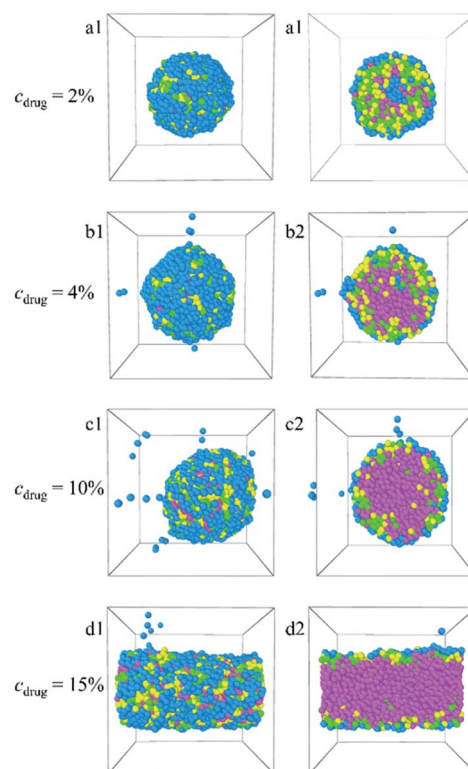

Fig. 8 Morphology snapshots (a1–d1) and their sectional view (a2–d2) of Dtx-loaded PLGA-b-PEG-b-PLGA micelles with different Dtx drug content. The green, yellow and blue spheres represent beads L, G, and E respectively, and the pink spheres represent beads D1, D2, and D3 of the Dtx drug.

different content of Dtx drugs are explored by DPD simulation, as shown in Fig. 8. The corresponding density distributions of E, L, G beads of the PLGA-b-PEG-b-PLGA copolymers and Dtx beads are shown in Fig. S8.† Here, the concentration of the PLGA$_3$-b-PEG$_7$-b-PLGA$_3$ copolymers is fixed as 10%, the content of the Dtx drugs is increased from 2% to 15%. When the content of the drug c_{drug} = 2% [Fig. 8a1, a2 and S8a†], an onionlike structure is observed with the Dtx drug beads distributed at the PLGA middle layer. With the content of the Dtx drugs increasing from c_{drug} = 4% to 10% [Fig. 8b1–c2 and S8b, c†], the Dtx drug beads are distributed at the center of the PLGA$_3$-b-PEG$_7$-b-PLGA$_3$ micelle and form the hydrophobic core, which is warped by the PLGA$_3$-b-PEG$_7$-b-PLGA$_3$ copolymer beads. The size of the micelle also grows gradually. When the content of the Dtx drug increases to c_{drug} = 15% [Fig. 8d1, d2 and S8d†], due to the combination of micelles and drug aggregates, the morphology of the micelle is not a spherical structure anymore, but a columnar structure with PLGA$_3$-b-PEG$_7$-b-PLGA$_3$ copolymers absorbed on the outer surface. These results indicate that as the content of the Dtx drugs is to be as high as a certain degree, to ensure the stability of micelles, the structure of Dtx-loaded PLGA$_3$-b-PEG$_7$-b-PLGA$_3$ micelle will change significantly.

3.3 The Dtx release process under shear flow

To investigate the release process of the Dtx drugs, we add the shear flow to the system. The concentration of the PLGA$_3$-b-PEG$_7$-b-PLGA$_3$ copolymers is fixed as 10%, the shear rates vary from 0.2 to 5. We found that as the shear rate ν < 3.5, the aggregate changes from a spherical micelle to a columnar structure [Fig. S9†]. When the shear rates $\nu \geq 3.5$, the Dtx drug will be released completely from the micelle. Fig. 9 shows the morphologies of the Dtx-loaded micelles at different simulation times under shear flow. In Fig. 9, we found that as the shear rate ν = 3.5, the spherical micelle rapidly changes to a columnar structure [Fig. 9a and b]. With the time evolution, the Dtx beads distribution in water increases, which indicates that Dtx drug

release from the carrier increases [Fig. 9c and d]. In the final state, at t > 15 000, the copolymers, Dtx drugs and water are randomly mixed, all Dtx drugs are released [Fig. 9e and f].

4. Conclusions

In this paper, the blank and drug-loaded polymeric micelles assembled from PLGA-b-PEG-b-PLGA copolymers and the mixture of PLGA-b-PEG-b-PLGA and docetaxel drugs are investigated by the dissipative particle dynamics (DPD) simulations. The morphologies and structures are dependent on the molecular parameters, such as the PLGA-b-PEG-b-PLGA copolymers concentration, composition, the Dtx drug content and the shear rate. Both the blank PLGA-b-PEG-b-PLGA polymeric micelle and the Dtx-loaded PLGA-b-PEG-b-PLGA micelle undergo the transition from spherical (core–shell) to onionlike (core–middle layer–shell) to columnar and lamellar structure with increasing the copolymer concentration from c_{cp} = 2.5% to 40%. The onionlike structures are comprised of the PEG hydrophilic core, the PLGA hydrophobic middle layer, and the PEG hydrophilic shell. As the structure of Dtx-loaded micelle varies from spherical core–shell structure to core–middle layer–shell onionlike structure, the distribution of the Dtx drugs diffuses from the core to the PLGA middle layer of the aggregate. As the PLGA-b-PEG-b-PLGA copolymer with PEG block length N_{PEG} < 7, the hydrophilic PEG blocks are unable to pack the hydrophobic PLGA completely whether the blank micelles or the Dtx-loaded micelles. Besides, the content of the Dtx drugs also affects the self-assembled structure. When the drug content is under a certain value, spherical structures are gained and their size of them grows up with the increase of the drug content. When the content of the Dtx drugs is to be as high as a certain degree, to ensure the stability of micelles, the structure of Dtx-loaded PLGA$_3$-b-PEG$_7$-b-PLGA$_3$ micelle will change significantly. The Dtx release process is also investigated by adding a shear flow along the x-axis. The morphologies of the Dtx-loaded micelles depend mainly on the shear rates, and with increasing the shear rates from 0.2 to 3.4, the spherical micelles turn into a cylindrical morphology. When the shear rate increases to 3.5, the Dtx drugs released gradually increase until all are released with time evolution.

Our investigations indicate that the structures and morphologies of the micelles are strongly correlated to the PLGA-b-PEG-b-PLGA copolymer concentration, composition, the Dtx drugs content, and the shear rate, which provides insights into the fundamental understanding of the Dtx-loaded PLGA-b-PEG-b-PLGA micelles systems. We hope this work could provide important theoretical guidance to design the new drug-loaded micelles.

Author contributions

Conceptualization, D. L.; methodology, D. L., M. W.; validation, D. L.; formal analysis, D. L.; resources, Y. L.; data curation, D. L., Y. L., M. W.; writing—original draft preparation, D. L.; writing—review and editing, D. L.; supervision, D. L., Y. L.; project
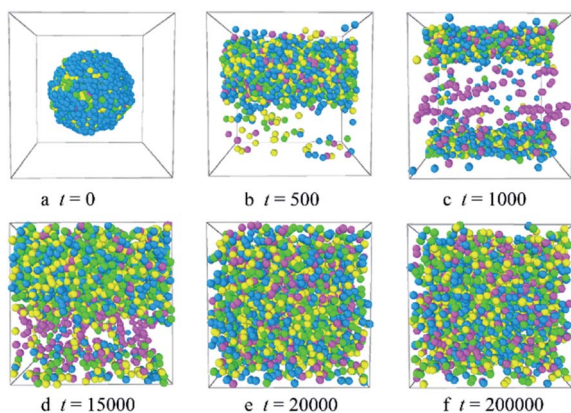

Fig. 9 Representative morphologies of Dtx-loaded PLGA$_3$-b-PEG$_7$-b-PLGA$_3$ micelles at different simulation times with shear rate 3.5. The green, yellow and blue spheres represent beads L, G, and E respectively, and the pink spheres represent beads D1, D2, and D3 of the Dtx drug.

administration, D. L., Y. L., M. W., J. G.; funding acquisition, Y. L., and D. L.

Conflicts of interest

There are no conflicts to declare.

Acknowledgements

Notes and references

1 H. Cabral, K. Miyata, K. Osada and K. Kataoka, *Chem. Rev.*, 2018, **118**, 6844.

2 S. Hossen, M. K. Hossain, M. K. Basher, M. N. H. Mia, M. T. Rahman and M. J. Uddin, *J. Adv. Res.*, 2019, **15**, 1.

3 J. K. Patra, G. Das, L. F. Fraceto, E. V. R. Campos, M. D. P. Rodriguez-Torres, L. S. Acosta-Torres, L. A. Diaz-Torres, R. Grillo, M. K. Swamy, S. Sharma, S. Habtemariam and H. S. Shin, *J. Nanobiotechnol.*, 2018, **16**, 71.

4 Z. X. Yang, H. Q. Zhao, D. L. Wang, L. Yin, K. X. Cai, Z. H. Lin, T. Chen and C. F. Yang, *Phys. Chem. Chem. Phys.*, 2021, **23**, 19011.

5 X. B. Wang, L. Wang, S. X. Yang, M. M. Zhang, Q. Q. Xiong, H. Y. Zhao and L. Liu, *Macromolecules*, 2014, **47**, 1999.

6 K. Fukushima, R. C. Pratt, F. Nederberg, J. P. K. Tan, Y. Y. Yang, R. M. Waymouth and J. L. Hedrick, *Biomacromolecules*, 2008, **9**, 3051.

7 F. Xu, J. W. Xu, B. X. Zhang and Y. L. Luo, *AIChE J.*, 2015, **61**, 35.

8 W. Xun, H. Y. Wang, Z. Y. Li, S. X. Cheng, X. Z. Zhang and R. X. Zhuo, *Colloids Surf., B*, 2011, **85**, 86.

9 Z. M. Song, R. L. Feng, M. Sun, C. Y. Guo, Y. Gao, L. B. Li and G. X. Zhai, *J. Colloid Interface Sci.*, 2011, **354**, 116.

10 D. E. Owens, *Int. J. Pharm.*, 2006, **307**, 93.

11 L. Yu, T. Y. Ci, S. C. Zhou, W. J. Zeng and J. D. Ding, *Biomater. Sci.*, 2013, **1**, 411.

12 L. Yu, G. T. Chang, H. Zhang and J. D. Ding, *Int. J. Pharm.*, 2008, **348**, 95.

13 G. T. Chang, T. Y. Ci, L. Yu and J. D. Ding, *J. Controlled Release*, 2011, **156**, 21.

14 G. T. Chang, C. Li, W. Y. Lu and J. D. Ding, *Macromol. Biosci.*, 2010, **10**, 1248.

15 G. M. Zentner, R. Rathi, C. Shih, J. C. McRea, M. H. Seo, H. Oh, B. G. Rhee, J. Mestecky, Z. Moldoveanu, M. Morgan and S. Weitman, *J. Controlled Release*, 2001, **72**, 203.

16 E. Khodaverdi, F. S. M. Tekie, S. A. Mohajeri, F. Ganji, G. Zohuri and F. Hadizadeh, *AAPS PharmSciTech*, 2012, **13**, 590.

17 A. Vonarbourg, C. Passirani, P. Saulnier and J. P. Benoit, *Biomaterials*, 2006, **27**, 4356.

18 S. Moffatt and R. J. Cristinao, *Int. J. Pharm.*, 2006, **317**, 10.

19 Y. Gao, F. Z. Ren, B. Y. Ding, N. Y. Sun, X. Liu, X. Y. Ding and S. Gao, *J. Drug Targeting*, 2011, **19**, 516.

20 S. B. Chen and J. Singh, *Int. J. Pharm.*, 2008, **352**, 58.

21 Y. M. Kwon and S. W. Kim, *Pharm. Res.*, 2004, **21**, 339.

22 C. Pratoomsoot, H. Tanioka, K. Hori, S. Kawasaki, S. Kinoshita, P. Tighe, J. H. Dua, K. M. Shakesheff and F. R. A. J. Rose, *Biomaterials*, 2008, **29**, 272.

23 L. Yu, Z. Zhang, H. Zhang and J. D. Ding, *Biomacromolecules*, 2009, **10**, 1547.

24 L. Yu, G. T. Chang, H. Zhang and J. D. Ding, *J. Polym. Sci., Part A: Polym. Chem.*, 2007, **45**, 1122.

25 N. K. Khorshid, K. Z. Zhu, K. D. Knudsen, S. Bekhradnia, S. A. Sande and B. Nyström, *Macromol. Biosci.*, 2016, **16**, 1838.

26 D. L. G. Cao, X. X. Zhang, M. Akabar, Y. Luo, H. Wu, X. Ke and T. Y. Ci, *Artif. Cells, Nanomed., Biotechnol.*, 2019, **47**, 181.

27 P. J. Hoogerbrugge and J. M. V. A. Koelman, *Europhys. Lett.*, 1992, **19**, 155.

28 R. D. Groot and K. L. Rabone, *Biophys. J.*, 2001, **81**, 725.

29 C. Yang, C. Yuan, W. Liu, J. Guo, D. Feng, X. Yin, W. Lin, P. S. Shuttleworth and H. Yue, *Colloids Surf., B*, 2019, **178**, 56.

30 S. Y. Nie, W. J. Lin, N. Yao, X. D. Guo and L. J. Zhang, *ACS Appl. Mater. Interfaces*, 2014, **6**, 17668.

31 Y. Wang, D. D. Zhu, J. Zhou, Q. L. Wang, C. Y. Zhang, Y. J. Liu, Z. M. Wu and X. D. Guo, *Colloids Surf., B*, 2015, **136**, 536.

32 M. M. Kuru, E. A. Dalgakiran and G. Kacar, *Colloids Surf., A*, 2021, **629**, 127445.

33 D. M. Liu, K. Gong, Y. Lin, T. Liu, Y. Liu and X. Z. Duan, *Polymers*, 2021, **13**, 1516.

34 D. M. Liu, K. Gong, Y. Lin, H. F. Bo, T. Liu and X. Z. Duan, *Polymers*, 2021, **13**, 2333.

35 D. M. Liu, M. Y. Yang, D. P. Wang, X. Y. Jing, Y. Lin and X. Duan, *Polymers*, 2021, **13**, 2866.

36 D. M. Liu, Y. Lin, K. Gong, H. F. Bo, D. Y. Li, Z. X. Zhang and W. D. Chen, *RSC Adv.*, 2021, **11**, 38316.

37 Y. H. Feng, X. P. Zhang, Z. Q. Zhao and X. D. Guo, *Mol. Pharmaceutics*, 2020, **17**, 1778.

38 B. Y. Li, Y. C. Li and Z. Y. Lu, *Polymer*, 2019, **171**, 1.

39 X. Y. Song, H. Guo, J. B. Ta, S. L. Zhao, X. Han and H. L. Liu, *Chem. Eng. Sci.*, 2018, **189**, 75.

40 T. Seki, N. Arai, D. Suh, T. Ozawa, T. Shimada, K. Yasuoka and A. Hotta, *RSC Adv.*, 2018, **8**, 26461.

41 X. D. Ma, Y. R. Zhou, L. S. Zhang, J. P. Lin and X. H. Tian, *Nanoscale*, 2018, **10**, 16873.

42 Y. Jin, D. Y. Guo, B. Li, S. P. Xu, J. Cheng, L. Li, X. F. Wen and P. H. Pi, *Phys. Chem. Chem. Phys.*, 2018, **20**, 4074.

43 A. Prhashanna and E. E. Dormidontova, *Macromolecules*, 2017, **50**, 1740.

44 A. Prhashanna and S. B. Chen, *Polymer*, 2017, **118**, 22.

45 A. J. Peters and T. P. Lodge, *Macromolecules*, 2017, **50**, 6303.

46 C. L. Wang, S. Y. Ma, Y. Hu and R. Wang, *Langmuir*, 2017, **33**, 3427.

47 J. J. Li, S. Y. Xiao, Y. X. Xu, S. Zuo, Z. S. Zha, W. D. Ke, C. X. He and Z. S. Ge, *ACS Appl. Mater. Interfaces*, 2017, **9**, 17727.

48 J. M. Borreguero, P. A. Pincus, B. G. Sumpter and M. Goswami, *Macromolecules*, 2017, **50**, 1193.

49 K. H. Myint, J. R. Brown, A. R. Shim, B. E. Wyslouzil and L. M. Hall, *J. Phys. Chem. B*, 2016, **120**, 11582.

50 S. Y. Ma, Y. Hu and R. Wang, *Macromolecules*, 2015, **48**, 3112.

51 N. K. Li, W. H. Fuss, L. Tang, R. P. Gu, A. Chilkoti, S. Zauscher and Y. G. Yingling, *Soft Matter*, 2015, **11**, 8236.

52 F. R. Cheng, X. W. Guan, H. Cao, T. Su, J. Cao, Y. W. Chen, M. T. Cai, B. He, Z. W. Gu and X. L. Luo, *Int. J. Pharm.*, 2015, **492**, 152.

53 R. D. Groot and P. B. Warren, *J. Chem. Phys.*, 1997, **107**, 4423.

54 R. Xu, M. A. Winnik, F. R. Hallett, G. Riess and M. D. Croucher, *Macromolecules*, 1991, **24**, 87.

55 A. Maiti and S. Mcgrother, *J. Chem. Phys.*, 2004, **120**, 1594.

56 X. D. Guo, J. P. K. Tan, L. J. Zhang, M. Khan, S. Q. Liu, Y. Y. Yang and Y. Qian, *Chem. Phys. Lett.*, 2009, **473**, 336.

57 Y. Cao, B. C. Wang, L. C. Yang, Y. Z. Wang and G. K. Singh, *J. Appl. Polym. Sci.*, 2015, **132**, 41280.

58 H. Y. Liu, H. Y. Guo and J. Zhou, *Acta Chim. Sin.*, 2012, **70**, 2445.

59 M. Wang, J. H. Zhan, L. J. Xu, Y. J. Wang, D. Lu, Z. Li, J. H. Li, F. Luo and H. Tan, *J. Biomater. Sci., Polym. Ed.*, 2020, **5**, 613.

60 Z. L. Luo and J. W. Jiang, *Polymer*, 2010, **51**, 291.

61 P. C. Sun, Y. H. Yin, B. H. Li, T. H. Chen, Q. H. Jin, D. T. Ding and A. C. Shi, *J. Chem. Phys.*, 2005, **122**, 204905.

62 M. Chansuna, N. Pimpha and V. Vao-soongnern, *J. Polym. Res.*, 2014, **21**, 452.